Title
Ambient-Pressure X-ray Photoelectron Spectroscopy Study of Cobalt Foil Model Catalyst under CO, H2, and Their Mixtures

Journal
ACS Catalysis, 7(2)

ISSN
2155-5435

Authors
Wu, Cheng Hao
Eren, Baran
Bluhm, Hendrik
et al.

Publication Date
2017-02-03

DOI
10.1021/acscatal.6b02835

Peer reviewed

An Ambient-Pressure X-ray Photoelectron Spectroscopy Study of Cobalt Foil Model Catalyst under CO, H_2, and their Mixtures

Cheng Hao Wu,[1,2] Baran Eren,[2] Hendrik Bluhm,[3] Miquel B. Salmeron[2,3,4,*]

[1] Department of Chemistry, University of California, Berkeley, CA 94720, USA
[2] Materials Sciences Division, Lawrence Berkeley National Laboratory, Berkeley, CA 94720, USA
[3] Chemical Sciences Division, Lawrence Berkeley National Laboratory, Berkeley, CA 94720, USA
[4] Department of Materials Science and Engineering, University of California, Berkeley, CA 94720, USA

*Email: mbsalmeron@lbl.gov

Abstract

Ambient-pressure XPS was used to investigate the reactions of CO, H_2, and their mixtures on Co foils. We found that CO adsorbs molecularly on the clean Co surface and desorbs intact in vacuum with increasing rate until ~90°C where all CO desorbs in seconds. In equilibrium with 100 mTorr gas, CO dissociates above 120°C, leaving carbide species on the surface but no oxides, because CO efficiently reduces the oxides at temperatures ~100°C lower than H_2. Water as impurities or produced by reaction of CO and H_2 efficiently oxidizes Co even at room temperature. Under 97:3 CO/H_2 mixture and with increasing temperatures, the Co surface becomes more oxidized and covered by hydroxyl groups until ~150°C where surface starts to get reduced, accompanied by carbide accumulation indicative of CO dissociation. Similar trend was observed for 9:1 and 1:1 mixtures but surface reduction begins at higher temperatures.

Keywords: Catalysis, Fischer-Tropsch Synthesis, Cobalt, Ambient-Pressure X-ray Photoelectron Spectroscopy

1. Introduction

Modern gas-to-liquid (GTL) technology aims to produce synthetic lubricants and liquid fuels from synthesis gas (or syngas for short, a mixture of carbon monoxide (CO), hydrogen (H_2), and often some carbon dioxide (CO_2)), which can be obtained from the conversion of coal, natural gas, and renewable biomass sources.[1–4] The Fischer-Tropsch (F-T) process consists of a series of reactions that catalytically convert syngas to long-chain hydrocarbons,[5,6] and plays an essential role in GTL technology, which has therefore attracted a great deal of scientific interest over the past few decades.[7–11]

Cobalt (Co) is among the best catalysts used in commercial F-T synthesis, thanks to its superior activity, high probability of chain growth, and low water-gas-shift activity (i.e., $CO + H_2O \leftrightarrow CO_2 + H_2$), although it is more expensive compared to iron, which is another commercially available catalyst.[4,7] In order to use the metal more efficiently and achieve optimal catalyst design, it is crucial to understand the fundamental processes taking place on the catalyst surface during F-T synthesis. For example, one of the elemental steps in F-T synthesis is the dissociation of adsorbed CO molecules. Two reaction pathways have been proposed and evaluated via theoretical calculations, namely the carbide mechanism and the hydrogen-assisted mechanism, both still under debate. The main difference between the two is whether or not hydrogen adsorbed on the catalyst surface participates in CO dissociation.[12–14] Other relevant processes of practical interest include carbon deposition, catalyst poisoning, short-term and long-term deactivation, catalyst regeneration, etc.[15–20]

Co-based F-T catalysts have been extensively studied in the past, including Co single crystals, polycrystalline Co foils, and Co nanoparticles on different oxide supports.[21] Many (surface science) characterization techniques,[4,21] such as scanning tunneling microscopy (STM),[16,22] various electron spectroscopies (e.g., x-ray photoelectron spectroscopy (XPS), Auger electron spectroscopy (AES), x-ray absorption spectroscopy (XAS)),[23–26] and temperature-programmed desorption (TPD),[24,27,28] have been very helpful in the mechanistic studies of various catalytic systems. In many cases, the chemical and structural changes of the Co catalyst surface were characterized *ex situ*, i.e., by comparing the catalyst before and after the reaction. More recently surface characterization techniques that work under more realistic conditions have been developed in an attempt to close the pressure gap between surface science and heterogeneous catalysis.[29–39] Ambient-pressure XPS (AP-XPS) is one successful example

for operation in the mTorr to few Torr range. Synchrotron light sources provide the additional advantages of high brilliance and variable x-ray energy, which facilitates efficient probing of the catalyst chemical state and the nature of adsorbed and dissolved species with different probing depths.[35,36,40]

In this article we used AP-XPS to systematically investigate the chemical state of a polycrystalline Co foil surface in the presence of pure CO and H_2 reactant gases and their mixtures.

2. Materials and Experimental Methods

The Co foil (Purity: 99.9%; Temper: as rolled) was purchased from Goodfellow Corporation. To minimize contamination, the gas lines for CO and H_2 were baked at 120°C and purged several times before pressurization. Prior to introduction of CO into the measurement chamber, the CO gas (Purity: 99.99%) was passed through a hot trap of copper beads at 250°C, to remove any carbonyl contaminants. We checked Ni XPS signal on a regular basis to make sure that no Ni deposition occurred during our experiments. Similarly, ultra-pure H_2 gas (99.999% purity) passed through a liquid nitrogen trap to minimize residual water impurities by freezing. As will be discussed later, H_2 introduction causes an increase in the background pressure of water, possibly because of reactions with the chamber walls which became more severe with time, as shown in the mass spectrometry measurement performed after three days of *in situ* measurements (Figure S1). Unfortunately background water is particularly problematic due to the high reactivity of Co with water to produce oxide.

AP-XPS measurements were carried out at the AP-XPS endstation of Beamline 11.0.2 of the Advanced Light Source (ALS) at the Lawrence Berkeley National Laboratory.[35] Before the experiments, the AP-XPS chamber was baked out at 120°C for 48hr, resulting in a base pressure of 1×10^{-9} Torr. *In situ* experiments were conducted within multiple 12-hour sessions, with 12-hour waiting period between each session. The base pressure could be recovered to low 10^{-9} Torr after 12-hour period. Before each set of measurements the Co foil was subject to a cleaning procedure in the preparation chamber (base pressure: 6×10^{-10} Torr) involving 1 keV Ar^+ sputtering, annealing to 400°C, heating in 1×10^{-7} Torr O_2 at 400°C, and again in vacuum at 700°C (details of these procedures are described in Section I of the supporting information (SI)). Repetition of this treatment

removed the surface carbon contamination, as verified by APXPS measurements. After the cleaning procedure the sample was intentionally exposed to a few mTorr of CO to cover its surface and prevent accumulation of background contaminants. This was not necessary in CO adsorption measurements conducted in the freshly annealed chamber, which had much less background water contamination. Sulfur and nitrogen were sometimes found on the Co surface. These contaminants impact CO adsorption on the Co surface as discussed in SI Section II. In all experiments presented below however, sulfur or nitrogen contamination was completely removed from the surface.

Unless otherwise noted, XPS spectra of each region were acquired with incident photon energies (E_{hv}) of 1000 eV for Co*2p*, 735 eV for O*1s*, and 490 eV for C*1s*, to produce ejected photoelectrons with kinetic energies (E_{kin}) of about 200 eV. According to electron inelastic mean free path (IMFP) data,[41] the probing depth of such photoelectrons is around 0.6 nm. To minimize beam damage, the x-ray beam was defocused and the shutter closed between measurements to block the x-ray beam from entering the measurement chamber. In addition, the beam spot was moved to a new location on the surface for each set of measurements. Unless otherwise noted, in all temperature-dependent measurements each set of spectra was acquired when the temperature of the Co foil stabilized at a target temperature with no more than ± 2°C fluctuation within approximately 20 min. Details about spectra fitting procedures are described in SI Section III.

3. Results and Discussion

3.1 Co surface after cleaning cycles

The survey XPS spectrum of the sample (Figure 1) acquired in ultra-high vacuum (UHV) while the surface was still at ~400°C, shows the chemical state of the surface after a cleaning cycle. Apart from the metal Co peaks only small C and O peaks are observed. Based on published ionization cross sections of each element[42] we estimate the concentration of these impurities to be below approximately 1% (atomic percentage or at%) with respect to Co. Percentage concentrations of surface species with respect to Co determined in this way will be used in the remaining of the paper. Details of the calculation method are described in SI Section III.

After the temperature decreased to RT following cleaning we obtained a nearly carbon-free surface, as shown by the C*1s* spectrum at the bottom of Figure 2a. The O*1s* spectrum

(shown in Figure 2b) however, exhibits an oxygen peak at 529.6 eV, which corresponds to approximately 10 at%. As will be discussed later this oxygen is likely the result of reaction between Co and residual H_2O in the UHV background. Since the Co*2p* spectrum (inset of Figure 1) does not exhibit features related to oxidized Co, we believe that the peak at 529.6 eV is related to adsorbed atomic oxygen.[27] There is also a small shoulder at 530.4 eV (<1 at%) due to an unidentified chemical species, which we will refer to as O_x. The intensity of the O_x species however almost never changed in the various chemical reactions studied below, indicating that it may correspond to a subsurface species.

3.2 CO adsorption and desorption on Co surface

Introduction of 1×10^{-5} mTorr CO into the chamber gave rise to new peaks at 285.5 eV and 531.6 eV in the C*1s,* and O*1s* regions of the XPS spectrum (Figure 2), respectively. They are attributed to CO molecules adsorbed on the metallic Co surface.[43] The asymmetry towards the higher binding energy (BE) side in the CO(ad) peaks, especially in the C*1s* region, is likely related to energy losses from excitation of electron-hole pairs and vibrational states of the adsorbed CO molecules.[44] Carbide species are also identified at ~283 eV.[17,45] An additional component at ~284 eV was needed to fit this region of the C*1s* spectra, probably corresponding to dissolved carbon in the subsurface region,[46] graphitic carbon, or hydrocarbons fragments, originating from beam-induced decomposition of gas phase CO, or from background hydrocarbon species.

When the CO pressure was increased to 10 mTorr, other than the adsorbed CO peaks, gas phase CO peaks around 290.5 eV and 537.0 eV (the exact positions depending on the sample work function (WF)) became clearly visible as shown in Figure 2, with increasing intensity under higher pressures of CO. It is noteworthy to mention that under 500 mTorr CO, the CO(ad) peaks in both C*1s* and O*1s* regions became noticeably broader: The full-width at half-maximum (fwhm) of CO(ad) peak increased to 0.94 eV in C*1s* spectrum and 1.61 eV in O*1s* spectrum, compared to 0.75 eV and 1.80 eV under low CO pressures. According to the TPD and XPS studies of CO adsorption on Co(0001),[18,24] CO molecules preferentially occupy top sites on the Co surface at low pressures, but will start to occupy other sites, such as bridge sites, at higher pressures. Similar phenomenon was also observed on surfaces like Ru(0001).[47] The broadening observed in the CO(ad) peaks therefore indicates a gradual increase in the occupancy alternative sites on the Co foil after the top sites become filled.

Quantitative comparison of apparent O*1s*/C*1s* ratio for adsorbed CO species (summarized in Table S1) revealed that at the lowest CO pressure tested here (1×10^{-5} mTorr), the O*1s*/C*1s* ratio (~1.6) is substantially higher than the ratio under higher pressure (1.1~1.3). This is probably due to OH groups present on the surface at low CO coverage. Unfortunately the O*1s* peaks of OH(ad) and CO(ad) are very close in BE making it difficult to distinguish these two species.

Upon evacuation of the 500 mTorr CO gas phase, about a third of adsorbed CO molecules (~6 at% wrt Co) remain on Co surface (Figure S2). To study the temperature dependence of CO desorption, the foil was heated at a rate of ~3°C/min while continuously recording XPS spectra in C*1s* region, as shown in Figure 3a. The temperatures reported in Figure 3a are those measured at the beginning of each spectrum. All spectra in the series were fitted with three components: i) CO(ad) at 285.5 eV, ii) carbon dissolved or CH_x groups (C(dis)/CH_x) around 284 eV, and iii) carbide species at ~283 eV. The intensity trend of each species is plotted against temperature in Figure 3b. The molecular CO disappeared almost completely around 90°C. This temperature is in line with the TPD measurements found in the literature.[18,24] The amount of C(dis)/CH_x remained constant, whereas the carbide peak slightly increased. The growth of carbide, although by a small amount (~1 at% after all CO molecules desorbed), is possibly associated with CO decomposition at defect sites, which can take place at temperatures as low as 330 K (57°C) according to Westsrate et al.[48]

3.3 CO dissociation on the metallic and oxidized Co surface

We have shown in the previous section that pure CO adsorbs and desorbs molecularly from the Co surface, desorption being fast (few seconds) and complete when the temperature reached 90°C. This indicates that the energy barrier for CO dissociation on metallic Co is higher than that for desorption. Therefore, to study the dissociation of CO the surface coverage should be maintained in equilibrium with the gas phase. We thus performed the experiment in the presence of 100 mTorr of CO gas.

The evolution of C*1s* spectra in this experiment is shown in Figure 4. With increasing temperature, the peak corresponding to adsorbed CO gradually decreased up to a temperature around 120°C, while the intensity of the carbide component remained almost unchanged. Above 120°C, however, a rapid increase of carbide peak intensity was

observed, indicative of CO dissociation. In addition to the increase in intensity, the line shape of the carbide peak became noticeably asymmetric, and an extra component centered at 0.6 eV lower BE was necessary to fit the peak (inset of Figure 4a). These two components could correspond to two different carbide species, one of them perhaps a more crystallized carbide[49] such as Co_2C identified in recent reports.[45,50] Besides these carbide peaks, the intensity of the component at 284 eV, assigned to C(dis)/CH_x, only slightly increased above 150^o. The observed increase in concentration of carbide species above 120°C cannot originate from beam-induced decomposition of gas phase CO, as beam effects should lead to a steady rate of carbide accumulation independent of the temperature. The onset temperature of direct CO dissociation around 120°C is the reason for introducing CO as a protecting agent during cooling below this particular temperature, as mention above, to minimize adsorption and contamination by background gases.

In the O*1s* region (spectra shown in Figure S3), a decrease in intensity of the CO(ad) peak (531.6 eV) was observed with increasing temperature paralleling the behavior of the corresponding 285.5 eV peak in the C*1s* region. The O(ad)/oxide component however did not increase compared to the initial value, indicative of no additional oxide formation. This also suggests that the oxygen atoms produced in the dissociation of CO most likely react with other CO molecules to form CO_2, which desorbs from the surface.[48,51] This result contradicts the conclusion by Lahtinen et al. that CO dissociation by itself can lead to oxidation of the Co surface and eventually deactivation of the Co catalyst.[52]

To investigate the interaction between CO and surface adsorbed oxygen and/or surface oxide in more detail, we intentionally oxidized Co by a brief exposure to 1×10^{-7} Torr of O_2 at RT. The Co*2p* spectrum (inset of Figure S4a) shows that the exposure led to oxidation of the majority (about 80%) of surface Co atoms. By fitting the Co*2p* spectrum and comparing the oxidized Co peak and its satellite features to the XPS spectra of standard compounds reported in the literature,[53] we determined that the oxidized Co species is most likely CoO.

After introduction of 100 mTorr of CO into the system, a *C1s* peak appeared 289 eV due to CO adsorbed on the oxide (CO(ad)@CoO_x), as shown in Figure 5a. This peak is considerably blue-shifted (3.5 eV) relative to that of CO on metallic Co, similar to the shift observed on oxidized copper.[54] In contrast, the O*1s* peak of CO adsorbed on the oxide has similar energy to that of CO(ad) on clean Co surface. Upon heating from RT no

substantial changes were observed in all O*1s* and C*1s* peaks until 150°C (Figure 5b and S4b). When the temperature reached 150°C, the *C1s* peak of CO(ad)@CoO_x at 289 eV started to decrease whereas the intensity of CO(ad) peak at 285.5 eV increased rapidly (Figures 5b and S4c). In the meantime the intensity of the oxide peak in O*1s* spectra decreased, indicating that surface oxide is being reduced by CO. At around 200°C, the surface was almost fully reduced to metallic Co. The surface reduction was also tracked by the percentage of Co^{x+} (Figure S4a). The reduction of the oxide is also accompanied by a shift of the C*1s* and *O1s* spectra of gas-phase CO towards lower (apparent) BE. The shifts indicated a decrease in the work function of the reduced surface (now covered by ~9 at% CO(ad) and ~15 at% carbide) relative to the oxidized Co surface.

Simultaneously with the reduction of the oxide, a rapid increase in the carbide concentration, and a mild growth of C(dis)/CH_x species were observed above 150^{o}C (Figure 5b). The chemical reduction of the oxidized Co surface by CO again disproves the conclusion that CO dissociation causes surface oxidation and catalyst deactivation. Contrary to our results, TPD studies on single crystal Co(0001) by Kizilkaya et al. revealed that the oxygen pre-covered Co surface cannot be reduced by CO (up to 1×10^{-5} Torr) within the temperature range of 100-500 K.[27] We attribute this discrepancy to the three orders of magnitude difference in CO pressure (10^{-2} Torr in our experiments vs 10^{-5} Torr in the TPD studies), which once again demonstrates the importance of studying catalyst surfaces under more realistic conditions.

3.4 Oxidation of Co by water impurities and reduction by H_2

As mentioned above and discussed further below, the introduction of H_2 generates background water, which is a very effective oxidant of Co (more details in SI Section V and in Figures S5-S8). Upon exposure to 100 mTorr of H_2, Co*2p* spectrum (bottom curve in Figure S5b) showed almost fully oxidized Co with prominent oxide satellite features. From the position of the main peak as well as the satellite features, the oxidized Co species is most likely CoO, possibly mixed with some $Co(OH)_2$, which cannot be easily distinguished in peak fittings.[53]

To study the reduction of Co oxide by H_2, the oxidized Co foil was heated in the presence of 100 mTorr H_2, while the O*1s* and Co*2p* spectra were monitored *in situ*. As shown in Figure S6a, adsorbed oxygen or surface oxide (O(ad)/oxide) kept growing until ~200°C

whereas the OH(ad) concentration dropped gradually. Beyond 200°C, both the oxide and OH(ad) peaks dropped rapidly and disappeared around 290°C, indicating complete reduction of Co surface and complete desorption of H_2O/OH(ad). Co*2p* spectra showed similar trend as shown in Figures S5b and S6b. Once the freshly reduced Co foil was cooled back to 185°C, still under 100 mTorr H_2, the surface was severally oxidized again (top spectrum in Figure S5b and the black square in Figure S6b). The oxide reduction experiments in CO and in H_2 demonstrate the substantially higher effectiveness of CO as a reducing agent, with a difference of nearly 100°C in onset temperature for reduction.

According to Kizilkaya *et al.*,[27] on the oxygen pre-covered Co (0001) surface H_2 does not react with surface oxygen at RT based on their TPD experiments. It is reported that under 2.3×10^{-5} Torr of H_2 the onset temperature for the reduction reaction is around 450 K (177°C) for flat Co(0001) and even higher (550 K or 277°C) for defective surfaces. The (full) reduction temperature from our experiments is in line with the value reported for the defective surfaces. The apparent activation barriers for water formation, was estimated using a simple kinetic model from these TPD data, as ~130 kJ/mol; therefore, oxygen removal via water formation can be considered as the rate-limiting step in the F-T reaction.[27,48] The effects of oxidation of Co by residual H_2O has serious consequences in practical catalytic reactions, not only because the industrial syngas may contain higher levels of water than the ultrapure H_2 gas used in research, but also because water is a by-product formed *in situ* on the catalyst surface. This may also be the main cause of catalyst oxidation in Co-based low-temperature F-T reactions.

3.5 Chemical state of Co surface under CO/H_2 mixtures

In the previous sections we presented results of reactions of CO and H_2 on Co separately. Here we focus on reactions involving CO/H_2 mixtures as those used in Fischer-Tropsch synthesis. As indicated above, we introduced CO first during cooling after the cleaning procedure (around 120^{o}C) in order to block the adsorption of background water and prevent the oxidation of the surface. After the temperature dropped to RT and CO partial pressure stabilized at desired values (97, 90, and 50 mTorr, respectively), H_2 was introduced to achieve a total pressure of 100 mTorr with three different CO:H_2 ratios of 97:3, 9:1, and 1:1.

Figure 6 shows the C*1s* and O*1s* XPS spectra collected at increasing temperatures from RT to 300°C, under 97 mTorr CO and 3 mTorr H_2. Because of the relatively low partial pressure of H_2, the Co surface was not appreciably oxidized at RT by background water in this case. When the temperature exceeded 50°C, the oxide peak in the O*1s* spectra grew substantially, as well as the component at 531.6 eV due to growing coverage of surface hydroxyl, the peak of which overlaps with that of CO(ad) in O*1s* spectra. The oxidation of Co is also corroborated by the growth of the peak at 289 eV in the C*1s* spectra related to the CO molecules adsorbed on oxidized Co, whereas peak intensity of CO(ad) on metallic Co at 285.5 eV decreased. In the meantime the concentration of residual carbide dropped slightly, possibly due to carbide decomposition in H_2 above 150°C,[50] which is even observable at RT as we discussed in SI (Section VI and Figure S9).

The intensity of the CO(ad)+OH(ad) component in the O*1s* region peaked at around 100°C, as the accumulation of reaction products H_2O and OH(ad) was balanced with increasing desorption rate at higher temperatures. Above 150°C the oxide peak decreased rapidly, indicating fast reduction primarily by CO. The reduction of Co was accompanied by an increase in the peak intensity of CO(ad) on metallic Co at 285.5 eV, and a decrease of the CO(ad)@CoO_x peak intensity at 289 eV. Meanwhile the intensities of the carbide peak and the C(dis)/CH_x component began to increase sharply, as a consequence of fast CO dissociation. At 200°C, the oxide peak in the O*1s* region shrank to a level smaller than the initial residual oxide peak, and all the adsorbed CO molecules resided on metallic Co surface.

The trends of surface species as a function of temperature under 97:3 CO/H_2 gas mixture, calculated from the fitting of C*1s* and O*1s* spectra, are summarized in Figures 7 and 8a. Assuming the intensity ratio of O*1s*/C*1s* signals from adsorbed CO molecules of 1.121 (the value at highest coverage of CO measured here, under 500 mTorr; see detailed explanation in SI section IV), the contribution of CO(ad) to the total intensity of the CO(ad)+OH(ad) peak can be calculated based on the combined C*1s* intensity of CO(ad) species (on both metallic and oxidized Co surface). The estimated O*1s* intensity of CO(ad), as well as that of OH(ad), as a function of temperature are shown by gray curves in Figure 8a.

The evolution of the chemical state of the Co foil surface can also be followed easily by the changes in the WF evidenced in the shift of CO(g) peaks in both C*1s* and O*1s* spectra,

as shown in Figures 7 and S10. From the direction of the shift we can conclude that the WF of metallic Co surface covered by CO is higher than the oxidized surface by 1.1eV. Once the surface is reduced at ~200°C, the WF dropped substantially (~0.8 eV), but the accumulation of surface carbide (~13 at% wrt Co at 250°C) increased the WF slightly (~0.2 eV).

Similar measurements were also performed under 9:1 and 1:1 CO/H_2 gas mixture. The evolution of surface species in these cases are also shown in Figures 7, 8b, and 8c. In the case of 9:1 CO/H_2 mixture, about 60% of the surface Co atoms were oxidized immediately after the introduction of H_2, estimated from the percentage of CO adsorbed on oxidized Co surface (Figure 8c). This percentage increased to about 80% in the case of 1:1 CO/H_2 mixture. Such rapid oxidation under higher H_2 partial pressure could be due to the rapid reaction or displacement of the adsorbed CO on the clean Co by H_2 even at RT as shown in the SI Section VI and Figure S9, leaving the reactive Co surface unprotected from the water molecules, both as a contaminant and reaction product. Upon heating, the general trends of the surface composition were similar to those in the case of 97:3 CO/H_2 mixture. Since CO is the more effective reducing agent as shown in the reduction experiments in CO and in H_2, the decrease in CO content (and increase of H_2 content) in the syngas mixture pushed up the onset temperature of surface reduction (~160°C and ~225°C in the cases of 9:1 and 1:1 CO/H_2 mixtures, respectively). Moreover, the accumulation of carbide and $C(dis)/CH_x$ species also began at higher temperatures with higher H_2 content, which is consistent with the report by Claeys et al.[50] The reasons for such trend of carbide accumulation are as following: 1) CO dissociation and carbide deposition is slower on oxidized Co and rapid accumulation of carbide only starts once the surface has been reduced to metallic state; 2) Carbide species rapidly decompose in H_2 above 150°C.[50] Higher H_2 content in the syngas mixture leads to higher onset temperature for surface reduction as well as higher rate of carbide decomposition, and both factors contribute to the higher onset temperatures of carbide accumulation.

In industrial practice, Co-based catalysts are used in low-temperature F-T reactions, at temperatures of 200-240°C in H_2 rich environment ($CO:H_2$ ~1:2).[4,48] The overall trend of surface evolution we observed in our *in situ* experiments indicates that the kinetic barrier for CO dissociation on oxidized Co surface is much higher than that on metallic Co surface; once the Co surface is reduced, CO dissociation can readily take place. Therefore the reduction of surface oxide is likely a rate-limiting step in the F-T reaction. When the

conversion rate of syngas is high in the F-T reactions, rapid water accumulation on the surface leads to oxidation and prevents further lowering of the reaction temperature for Co-catalyzed F-T processes. On the other hand, although reactions at higher temperature favors water/hydroxyl desorption and maintaining metallic Co surface, they also lead to the rapid accumulation of surface carbide, which has been shown to favor methane production over long-chain hydrocarbons.[50,55,56] To achieve optimum activity and selectivity of Co-based catalysts in the low-temperature F-T processes, it is best to maintain a metallic surface without high concentration of surface carbide species.

4. Conclusions

In summary, we used AP-XPS to investigate a polycrystalline Co foil as a model catalyst for F-T synthesis under pure CO, pure H_2, and different mixtures of CO and H_2 at various temperatures, aiming to observe the chemical evolutions of the Co surface *in situ* and *operando*.

We found that adsorbed CO on the clean Co surface desorbs completely around 90°C under vacuum, with no obvious dissociation. In the presence of 100 mTorr CO, direct CO dissociation takes place on clean Co surface only above 120°C, leaving a substantial amount of carbide species and some C(dis)/CH_x species on the surface. The metallic Co surface gets easily oxidized by water either as a background impurity or as a by-product of the hydrogenation reaction. The oxidized Co surface can be reduced by CO much more efficiently than by H_2, which requires a temperature higher by ~100°C to achieve full reduction.

Under the syngas mixture at RT, Co surface was oxidized with the extent of oxidation depending on the H_2 content in the mixture. As the temperature increases the Co surface gets oxidized further, but is eventually reduced rapidly at higher temperatures. The reduction temperatures also depend on the H_2 partial pressure in the syngas mixture. These trends are likely related to the relative ineffectiveness of surface reduction by H_2 compared to CO, as well as to the higher water production rate with high H_2 content. Once the surface is reduced, adsorbed CO molecules start to dissociate rapidly when the temperature rises further, leaving substantial accumulation of carbide species on the catalyst surface, which may shift the selectivity of the catalyst towards methane production.

It is worth mentioning that the working pressure in the above-mentioned experiments was typically 100 mTorr, which is much lower than that in practical F-T synthesis (typically tens of atmospheres). In industrial F-T synthesis, fast chain growth would lead to accumulation of liquid or wax species on the catalyst surface, which is unlikely to take place under the conditions in our experiments. Nevertheless, our results still provide useful reference information regarding the chemical states and evolutions of the catalyst surface in equilibrium with the syngas mixture.

Associated Content

Supporting Information

Detailed cleaning procedure of Co foils; Spectra fitting procedures and atomic ratio calculations; Discussion about control experiments including CO adsorption on poisoned Co foils, surface oxidation by water impurities, and titrating pre-adsorbed CO with H_2; Additional table and figures. This material is available free of charge via the Internet at http://pubs.acs.org.

Author Information

Corresponding author
*Email: mbsalmeron@lbl.gov

Notes

The authors declare no competing financial interest.

Acknowledgements

This work was supported by the Office of Basic Energy Sciences (BES), Division of Materials Sciences and Engineering, of the U.S. Department of Energy (DOE) under contract no. DE-AC02-05CH11231, through the Chemical Sciences, Geosciences, and Biosciences Division. Funding from the same contract for the ALS and beamline 11.0.2 is also acknowledged.

References

(1) Wender, I. *Fuel Process. Technol.* **1996**, *48*, 189–297.

(2) Schulz, H. *Appl. Catal. A Gen.* **1999**, *186*, 3–12.

(3) Geerlings, J. J. C.; Wilson, J. H.; Kramer, G. J.; Kuipers, H. P. C. E.; Hoek, A.; Huisman, H. M. *Appl. Catal. A Gen.* **1999**, *186*, 27–40.

(4) Khodakov, A. Y.; Chu, W.; Fongarland, P. *Chem. Rev.* **2007**, *107*, 1692–1744.

(5) Fischer, F.; Tropsch, H. *Brennstoff-Chemie* **1923**, *4*, 276–285.

(6) Van Der Laan, G. P.; Beenackers, A. A. C. M. *Catal. Rev.* **1999**, *41*, 255–318.

(7) Iglesia, E. *Appl. Catal. A Gen.* **1997**, *161*, 59–78.

(8) Dry, M. E. *Catal. Today* **2002**, *71*, 227–241.

(9) Torres Galvis, H. M.; Bitter, J. H.; Khare, C. B.; Ruitenbeek, M.; Dugulan, A. I.; de Jong, K. P. *Science* **2012**, *335*, 835–838.

(10) Torres Galvis, H. M.; De Jong, K. P. *ACS Catal.* **2013**, *3*, 2130–2149.

(11) Jiao, F.; Li, J.; Pan, X.; Xiao, J.; Li, H.; Ma, H.; Wei, M.; Pan, Y.; Zhou, Z.; Li, M.; Miao, S.; Li, J.; Zhu, Y.; Xiao, D.; He, T.; Yang, J.; Qi, F.; Fu, Q.; Bao, X. *Science* **2016**, *351*, 1065–1068.

(12) Shetty, S.; van Santen, R. A. *Catal. Today* **2011**, *171*, 168–173.

(13) Mitchell, W.; Xie, J. *J. Am. Chem. Soc.* **1995**, *7502*, 2606–2617.

(14) Shetty, S.; Jansen, A. P. J.; van Santen, R. A. *J. Am. Chem. Soc.* **2009**, *131*, 12874–12875.

(15) Lee, D. K.; Lee, J. H.; Ihm, S. K. *Appl. Catal.* **1988**, *36*, 199–207.

(16) Weststrate, C. J.; Kazalkaya, A. C.; Rossen, E. T. R.; Verhoeven, M. W. G. M.; Ciobîcă, I. M.; Saib, A. M.; Niemantsverdriet, J. W. *J. Phys. Chem. C* **2012**, *116*, 11575–11583.

(17) Fei Tan, K.; Xu, J.; Chang, J.; Borgna, A.; Saeys, M. *J. Catal.* **2010**, *274*, 121–129.

(18) Habermehl-Ćwirzeń, K.; Lahtinen, J. *Surf. Sci.* **2004**, *573*, 183–190.

(19) Tsakoumis, N. E.; Rønning, M.; Borg, Ø.; Rytter, E.; Holmen, A. *Catal. Today* **2010**, *154*, 162–182.

(20) Rytter, E.; Holmen, A. *Catalysts* **2015**, *5*, 478–499.

(21) Wang, Z.; Yan, Z.; Liu, C.; Goodman, D. W. *ChemCatChem* **2011**, *3*, 551–559.

(22) Wilson, J.; de Groot, C. *J. Phys. Chem.* **1995**, *99*, 7860–7866.

(23) Cabeza, G. F.; Légaré, P.; Castellani, N. J. *Surf. Sci.* **2000**, *465*, 286–300.

(24) Lahtinen, J.; Vaari, J.; Kauraala, K. *Surf. Sci.* **1998**, *418*, 502–510.

(25) Greuter, F.; Heskett, D.; Plummer, E. W.; Freund, H.-J. *Phys. Rev. B* **1983**, *27*.

(26) Wang, Z.; Skiles, S.; Yang, F.; Yan, Z.; Goodman, D. W. *Catal. Today* **2012**, *181*, 75–81.

(27) Kizilkaya, A. C.; Niemantsverdriet, J. W.; Weststrate, C. J. *J. Phys. Chem. C* **2016**, *120*, 4833–4842.

(28) van Helden, P.; van den Berg, J.-A.; Weststrate, C. J. *ACS Catal.* **2012**, *2*, 1097–1107.

(29) Ehrensperger, M.; Wintterlin, J. *J. Catal.* **2014**, *319*, 274–282.

(30) Ehrensperger, M.; Wintterlin, J. *J. Catal.* **2015**, *329*, 49–56.

(31) Tao, F.; Dag, S.; Wang, L.-W.; Liu, Z.; Butcher, D. R.; Bluhm, H.; Salmeron, M.; Somorjai, G. A. *Science* **2010**, *327*, 850–853.

(32) Eren, B.; Zherebetskyy, D.; Patera, L. L.; Wu, C. H.; Bluhm, H.; Africh, C.; Wang, L.-W.; Somorjai, G. A.; Salmeron, M. *Science* **2016**, *351*, 475–478.

(33) Zheng, H.; Smith, R. K.; Jun, Y.-W.; Kisielowski, C.; Dahmen, U.; Alivisatos, A. P. *Science* **2009**, *324*, 1309–1312.

(34) Zheng, H.; Meng, Y. S.; Zhu, Y. *MRS Bull.* **2015**, *40*, 12–18.

(35) Ogletree, F. D.; Bluhm, H.; Hebenstreit, E. D.; Salmeron, M. *Nucl. Instruments Methods Phys. Res. Sect. A Accel. Spectrometers, Detect. Assoc. Equip.* **2009**, *601*, 151–160.

(36) Salmeron, M.; Schlogl, R. *Surf. Sci. Rep.* **2008**, *63*, 169–199.

(37) Beitel, G. A.; de Groot, C. P. M.; Oosterbeek, H.; Wilson, J. H. *J. Phys. Chem. B* **1997**, *101*, 4035–4043.

(38) Chen, P.; Kung, K. Y.; Shen, Y. R.; Somorjai, G. A. *Surf. Sci.* **2001**, *494*, 289–297.

(39) Chen, P.; Westerberg, S.; Kung, K. Y.; Zhu, J.; Grunes, J.; Somorjai, G. A. *Appl. Catal. A Gen.* **2002**, *229*, 147–154.

(40) Starr, D. E.; Liu, Z.; Hävecker, M.; Knop-Gericke, A.; Bluhm, H. *Chem. Soc. Rev.* **2013**, *42*, 5833–5857.

(41) Powell, C. J.; Jablonski, A. *NIST Electron Inelastic Mean Free Path Database, version 1.1*; National Institute of Standards and Technology: Gaithersburg, MD, 2002.

(42) Yeh, J.; Lindau, I. *At. Data Nucl. Data Tables* **1985**, *32*, 1–155.

(43) Moyes, R. B.; Roberts, M. W. *J. Catal.* **1977**, *49*, 216–224.

(44) Smedh, M.; Beutler, A.; Ramsvik, T.; Nyholm, R.; Borg, M.; Andersen, J. N.; Duschek, R.; Sock, M.; Netzer, F. P.; Ramsey, M. G. *Surf. Sci.* **2001**, *491*, 99–114.

(45) Böller, B.; Ehrensperger, M.; Wintterlin, J. *ACS Catal.* **2015**, *5*, 6802–6806.

(46) Weatherup, R. S.; Amara, H.; Blume, R.; Dlubak, B.; Bayer, B. C.; Diarra, M.; Bahri, M.; Cabrero-Vilatela, A.; Caneva, S.; Kidambi, P. R.; Martin, M.-B.; Deranlot, C.; Seneor, P.; Schloegl, R.; Ducastelle, F.; Bichara, C.; Hofmann, S. *J. Am. Chem. Soc.* **2014**, *136*, 13698–13708.

(47) Starr, D. E.; Bluhm, H. *Surf. Sci.* **2013**, *608*, 241–248.

(48) Weststrate, C. J.; Van Helden, P.; Van De Loosdrecht, J.; Niemantsverdriet, J. W. *Surf. Sci.* **2016**, *648*, 60–66.

(49) Nagakura, S. *J. Phys. Soc. Japan* **1961**, *16*, 1213–1219.

(50) Claeys, M.; Dry, M. E.; Van Steen, E.; Du Plessis, E.; Van Berge, P. J.; Saib, A. M.; Moodley, D. J. *J. Catal.* **2014**, *318*, 193–202.

(51) Nakano, H.; Ogawa, J.; Nakamura, J. *Surf. Sci.* **2002**, *514*, 256–260.

(52) Lahtinen, J.; Anraku, T.; Somorjai, G. A. *Catal. Letters* **1994**, *25*, 241–255.

(53) Biesinger, M. C.; Payne, B. P.; Grosvenor, A. P.; Lau, L. W. M.; Gerson, A. R.; Smart, R. S. C. *Appl. Surf. Sci.* **2011**, *257*, 2717–2730.

(54) Eren, B.; Heine, C.; Bluhm, H.; Somorjai, G. A.; Salmeron, M. *J. Am. Chem. Soc.* **2015**, *137*, 11186–11190.

(55) Gruver, V.; Zhan, X.; Engman, J.; Robota, H. J.; Suib, S. L.; Polverejan, M. *Prepr. Pap.-Am. Chem. Soc. Div. Pet. Chem.* **2004**, *49*, 192.

(56) Moodley, D. J.; Van De Loosdrecht, J.; Saib, A. M.; Niemantsverdriet, J. W. In *Advances in Fischer-Tropsch Synthesis, Catalysts and Catalysis*; Davis, B. H.; Ocelli, M. L., Eds.; Taylor & Francis: Boca Raton, Florida, 2009; p. 49.

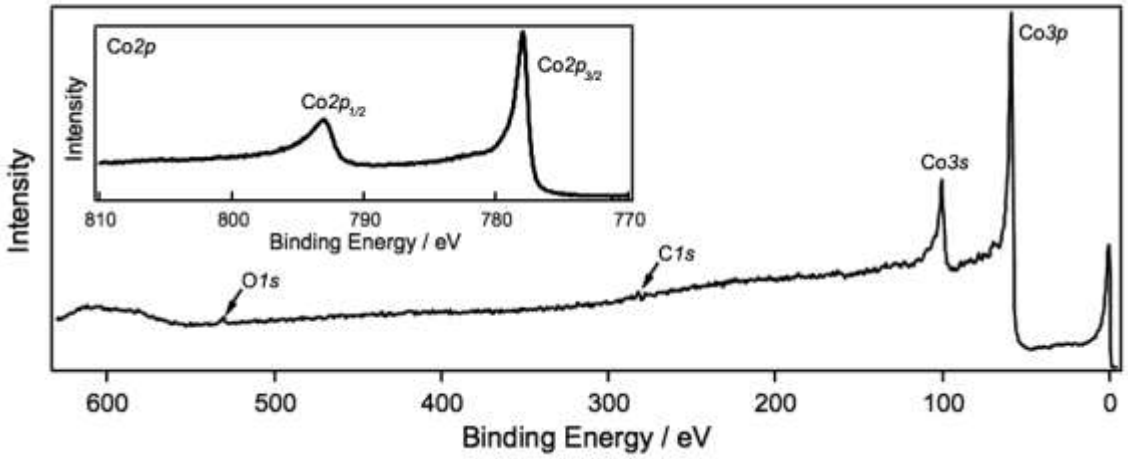

Figure 1. The survey spectrum of the cobalt foil surface after cleaning procedures (acquired at ~400°C, E_{hv} = 735 eV). The inset shows the Co*2p* region after cooling down to RT with E_{hv} = 1000 eV.

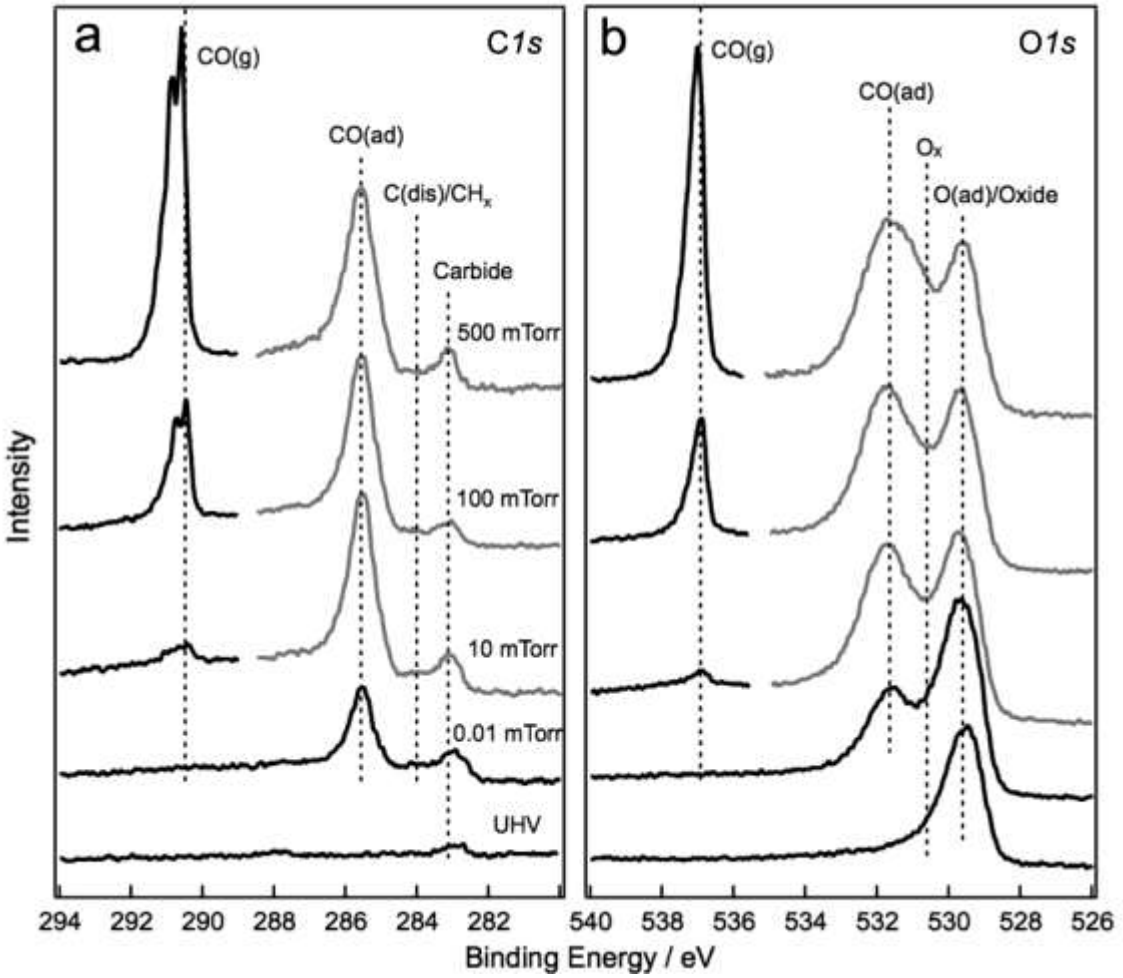

Figure 2. Pressure-dependent CO adsorption on cobalt foil surface. (a) C*1s* and (b) O*1s* regions of XPS spectra acquired with photon energies of 490 eV and 735 eV, respectively. The grey portion of the spectra were rescaled to compensate for gas attenuation of the electron flux. The attenuation coefficients were determined by comparing C*1s* peak intensities (E_{hv} = 490 eV) of an HOPG sample in UHV and under different pressures of CO.

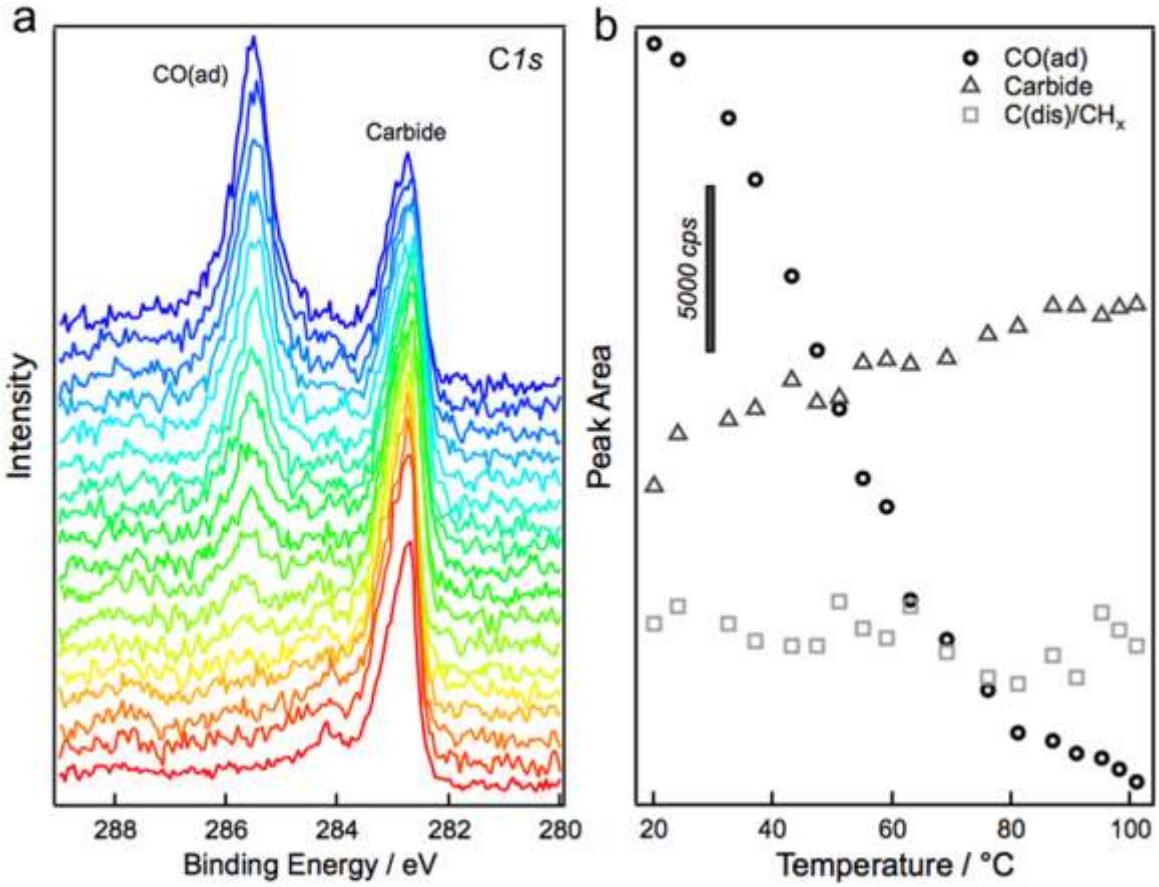

Figure 3. CO desorption from the cobalt surface. (a) C*1s* XPS spectra acquired in vacuum (E_{hv} = 490 eV). The colors of spectra from blue to red represent temperatures from RT to 101°C. (b) Peak areas of adsorbed CO (CO(ad)), carbide, and dissolved carbon (C(dis)) or hydrocarbon contaminants (CH_x) as a function of temperature, based on the peak fitting results from (a).

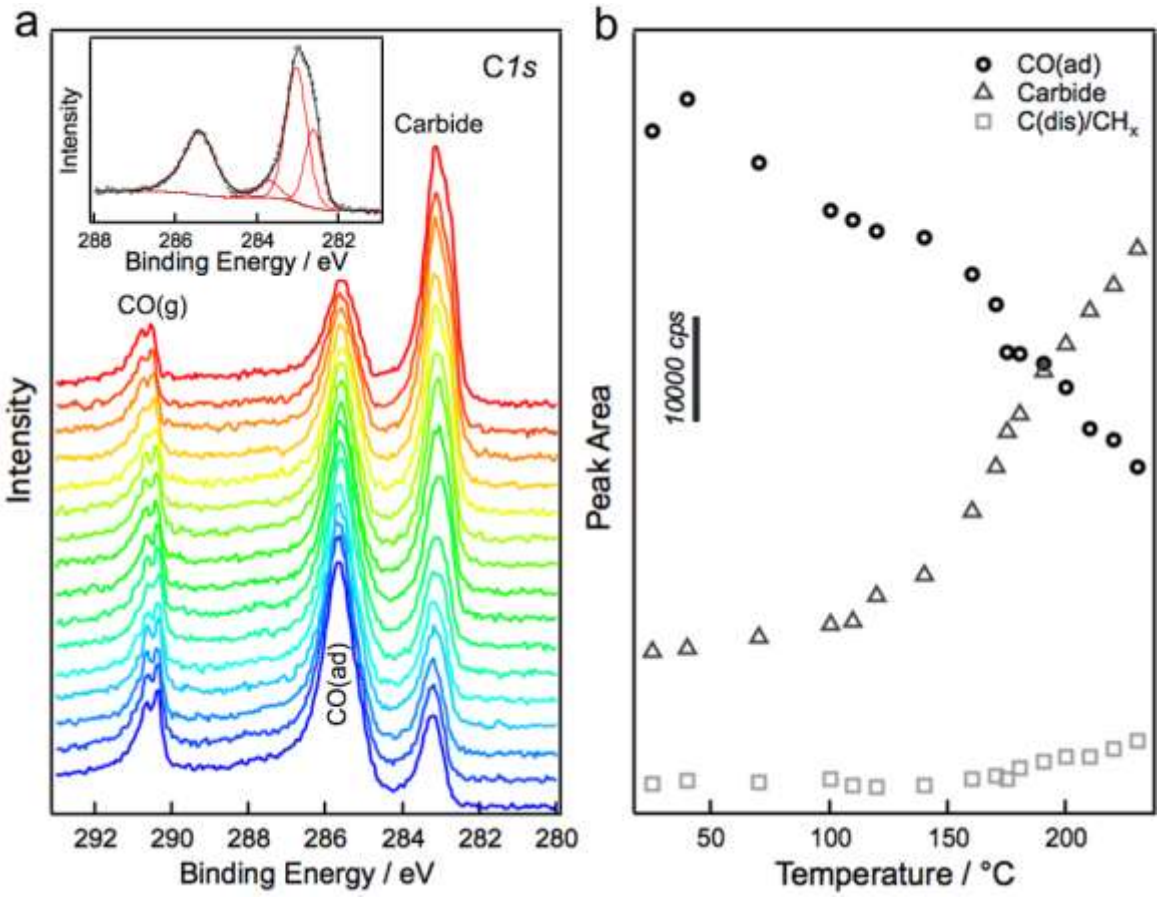

Figure 4. Thermally induced CO dissociation on the cobalt surface. (a) C*1s* XPS spectra (E_{hv} = 490 eV) under 100 mTorr CO. The colors of the spectra, from blue to red, represent temperatures from RT to 230°C. The inset shows the fitting of the C1s spectrum (gas phase region not included) acquired at 230°C showing components assigned to C(dis)/CH_x (~284 eV), two carbide species at 283 and 282.4 eV, and CO(ad) at 285.5 eV. (b) Peak areas of adsorbed CO, carbide, and dissolved carbon as a function of temperature, based on the peak fitting results from (a).

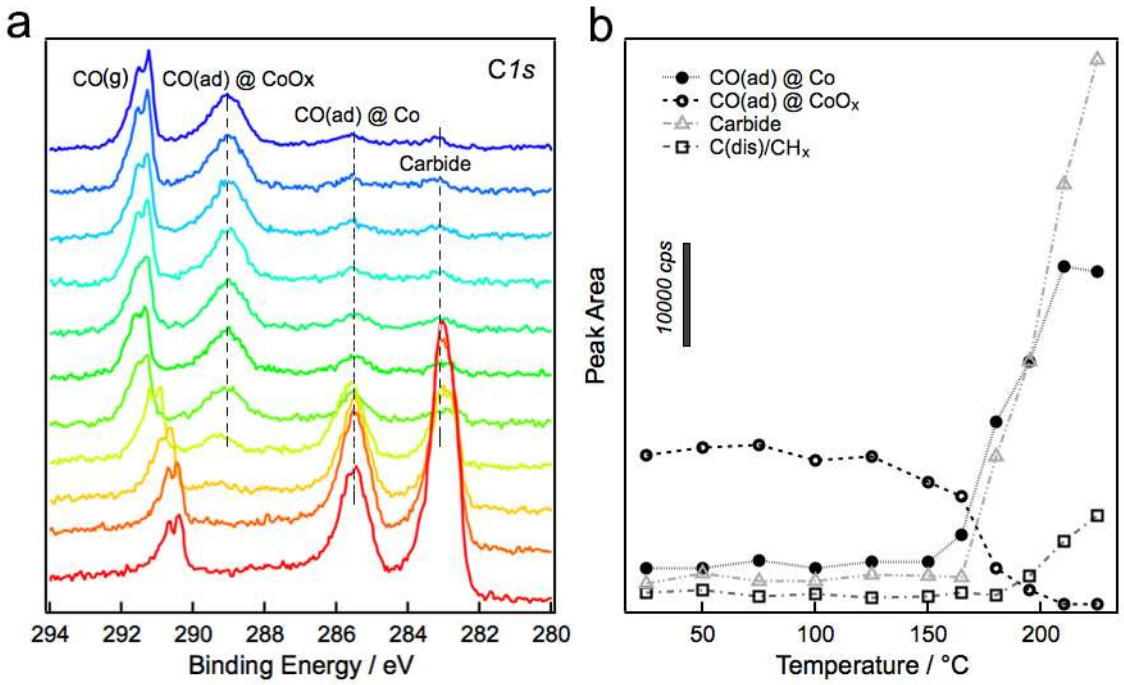

Figure 5. Reduction of surface Co oxide by CO. (a) C*1s* spectra (E_{hv} = 490 eV) acquired under 100 mTorr CO. The colors of spectra, from blue to red, represent temperatures from RT to 225°C. Molecular CO produces peaks from gas phase species (291.3 to 290.5 eV), and adsorbed species on metallic Co (285.5 eV), and on oxidized Co (289.0 eV). (b) Peak areas of adsorbed CO on metallic Co (CO(ad) @ Co) and on oxidized cobalt (CO(ad) @ CoO_x), carbide, and C(dis)/CH_x as a function of temperatures, based on the peak fitting results from (a).

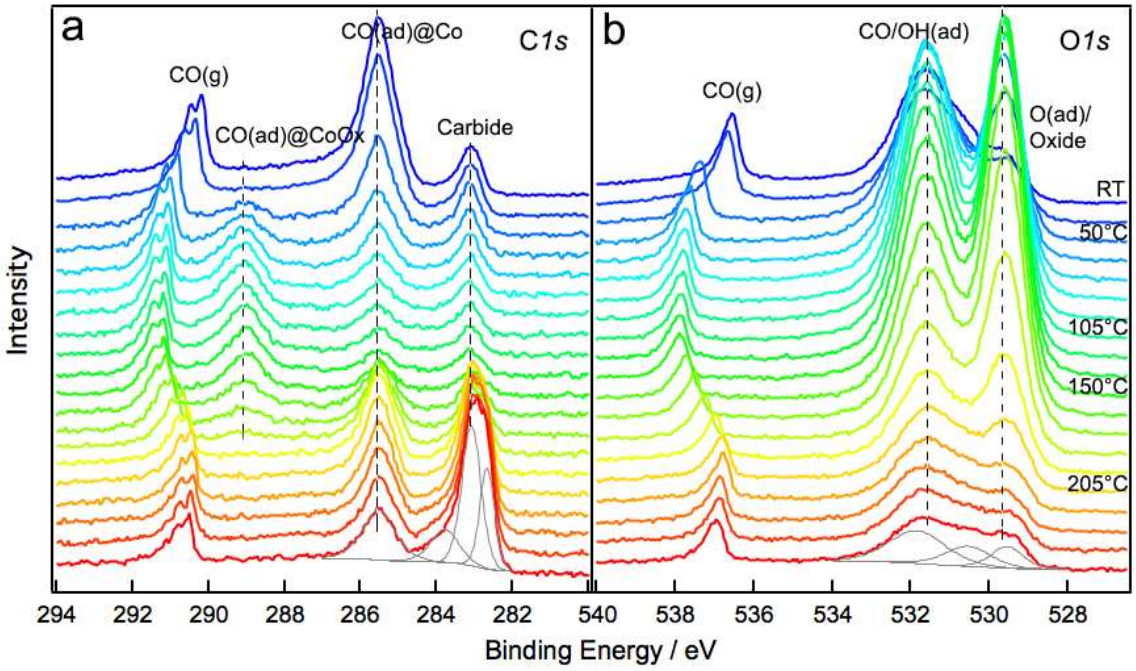

Figure 6. Evolution of the Co surface during reaction conditions under 97 mTorr CO and 3 mTorr H_2. (a) C*1s* and (b) O*1s* regions of XPS spectra as a function of temperatures. The colors of spectra, from blue to red, represent temperatures from RT to 250°C.

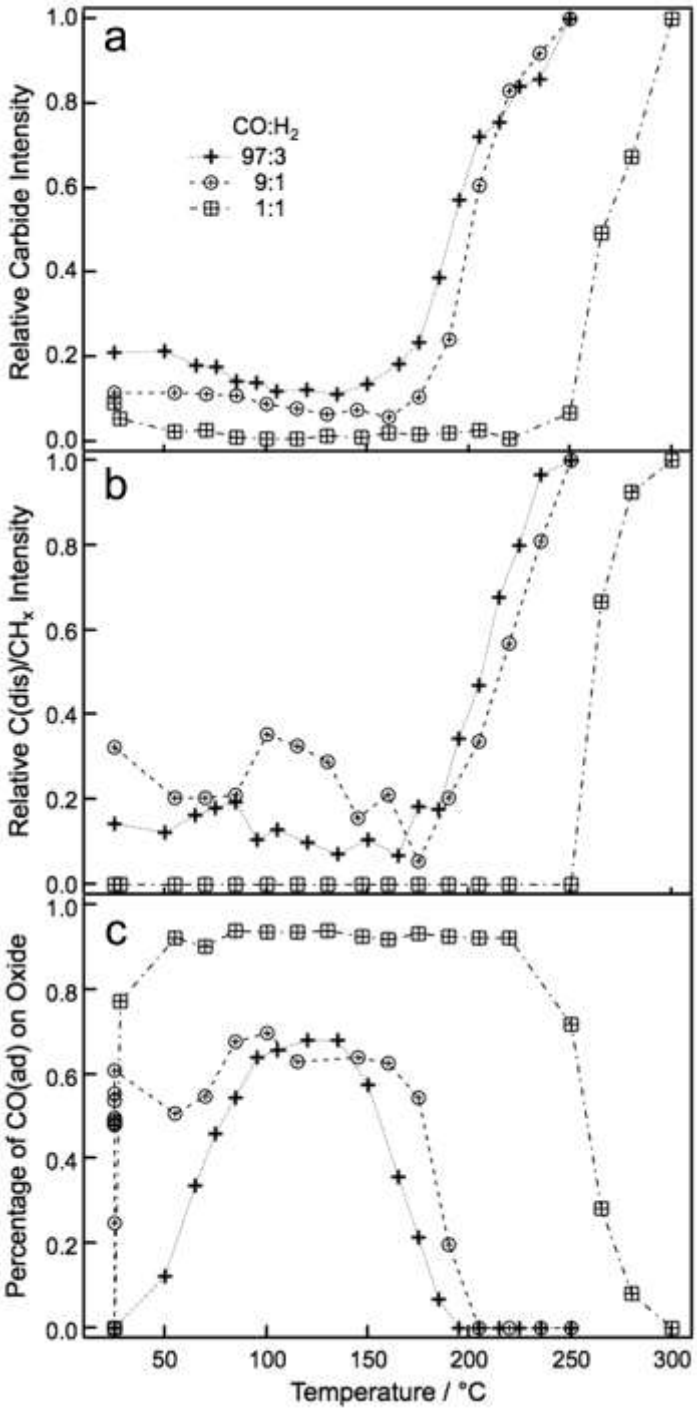

Figure 7. Relative concentration of surface species during reaction under mixtures of O and H_2. (a) carbide, (b) C(dis)/CH_x, and (c) adsorbed CO on oxidized cobalt as a function of temperature under 100 mTorr of gas mixture with three different CO:H_2 ratios (97:3, 9:1, and 1:1). In figure (a) and (b), for each CO/H_2 ratio, the peak intensities of carbide and C(dis)/CH_x species in the spectrum acquired at the highest temperatures were set to unity.

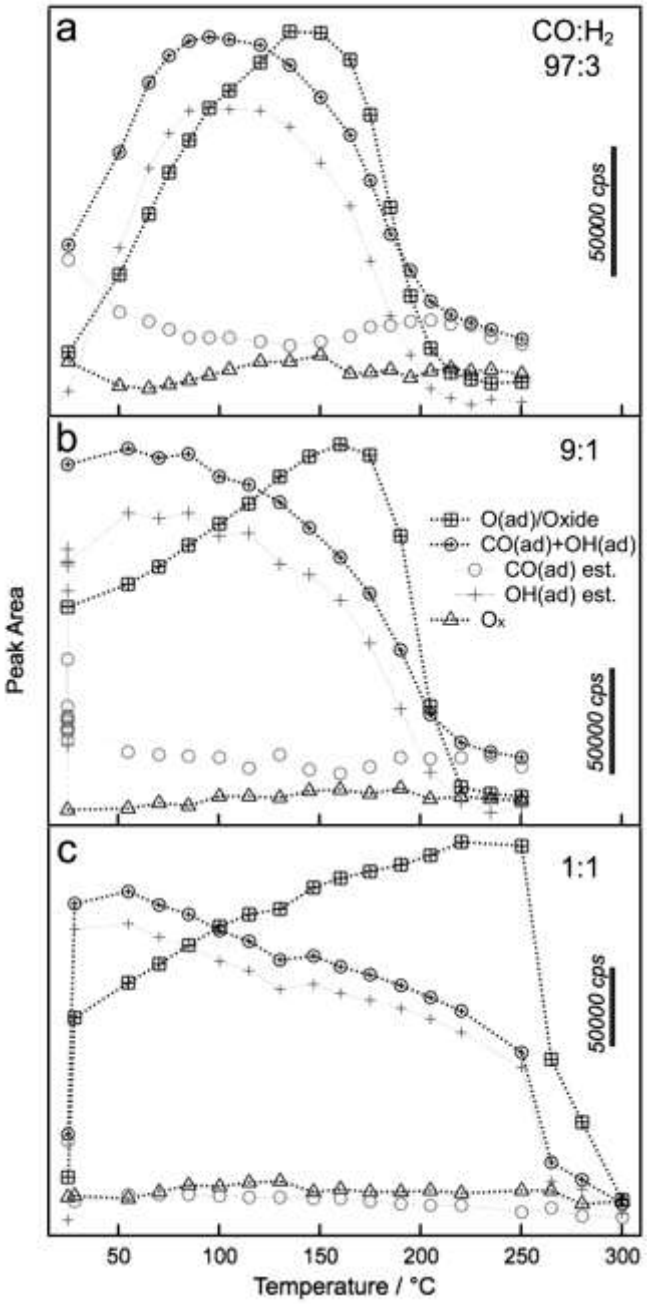

Figure 8. Evolution of the O(ad)/oxide, CO(ad), OH(ad), and O_x XPS peak areas as a function of temperature under 100 mTorr of CO/H_2 mixture with three different ratios: (a) 97:3, (b) 9:1, and (c) 1:1. The peak areas of O(ad)/oxide, O_x, and CO(ad)+OH(ad) were calculated from the fitting results of O*1s* spectra acquired under each condition (E_{hv} = 735 eV). The intensities of CO(ad) were estimated using the CO(ad) intensities in the corresponding C1s spectra, assuming that the O*1s*/C*1s* ratio of CO(ad) is 1.121 (see explanations in SI Section IV). The OH(ad) intensities were estimated by subtracting CO(ad) intensities from the corresponding total intensities of both.